Electronic Supplementary Material (ESI) for Materials Horizons.

Zn_2SbN_3: growth and characterization of a metastable photoactive material.

Elisabetta Arca[1]*, John D. Perkins[1], Stephan Lany[1], Allison Mis[1,2], Bor-Rong Chen[3], Patricia Dippo[1], Jonathan Partridge[1,4], Wenhao Sun[5], Aaron Holder[1,6], Adele C. Tamboli[1], Michael F. Toney[3,7], Laura T. Schelhas[7], Gerbrand Ceder[5,8], William Tumas[1], Glenn Teeter[1] and Andriy Zakutayev[1]*

[1] Materials Science Center National Renewable Energy Laboratory, Golden, Colorado 80401, United States

[2] Department of Metallurgical and Materials Engineering, Colorado School of Mines, Golden, Colorado 80401, United States

[3] Stanford Synchrotron Light Source, SLAC National Accelerator Laboratory, Menlo Park, CA, 94025, USA

[4] Department of Chemistry and Biochemistry, The University of Texas at Austin, Austin, Texas, 78705, United States

[5] Materials Science Division, Lawrence Berkeley National Laboratory, Berkeley, California 94720, United States

[6] Department of Chemical and Biological Engineering, University of Colorado Boulder, Boulder, Colorado 80309, United States

[7] Applied Energy Programs, SLAC National Accelerator Laboratory, Menlo Park, CA, 94025, USA

[8] Department of Materials Science and Engineering, University of California Berkeley, Berkeley, California 94720, United States

*Corresponding authors: Elisabetta.Arca@nrel.gov, Andriy.Zakutayev@nrel.gov

Supporting Information

S1 – Theoretical predictions.

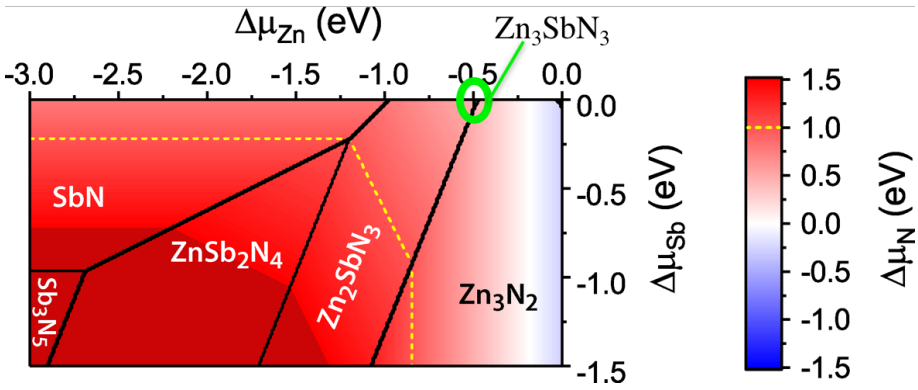

Figure SI1 Stability phase diagram of the possible Zn-Sb-N phases as determined by the KLM.

A data-mined structure prediction (DMSP) algorithm was used to identify new ternary nitrides. The stability of the candidate crystal structures was assessed by comparing their density functional theory (DFT) formation energies to the competing phases. 942 ternary metal-nitride chemical spaces were searched. Zn_2SbN_3 was identified as a candidate phase. To sample more comprehensively the Zn-Sb-N ternary space for possible compositions and their structures, we used the Kinetically Limited Minimization (KLM) approach[1]. This search was performed for many $Zn_iSb_jN_k$ chosen to accommodate the Zn^{2+}, $Sb^{3+/5+}$, and N^{3-} oxidation states. A KLM search was also performed for the Sb nitrides SbN and Sb_3N_5 which are so far unknown. As the competing phases, we considered known materials Zn_3N_2 (space group SG 206), ZnSb (SG 61), $Zn_{13}Sb_{10}$ (SG 2). The symmetry analysis for all structures was performed with the FINDSYM software[2]. The Crystallographic Information Files (CIF) were loaded into the MAUD program to simulate the reference XRD pattern. CIF files for all new stable structures are provided as Supporting Information.

The first-principles calculations in DFT and in the GW approximation were performed with the VASP code[3, 4]. The compound enthalpy of formation was calculated using fitted elemental reference energies[5]. The GW calculations were performed as described in Ref [6] and the optical absorption spectrum was calculated within the independent particle approximation.[7]

The crystal structure predictions identified three new ternary phases in the chemical space composed by Zn, Sb and N (Figure SI1): the $ZnSb_2N_4$ phase (SG 227), Zn_2SbN_3 (SG 36) and Zn_3SbN_3 (SG 8). Additionally, a new metastable binary antimony nitride phase SbN (SG 29) is predicted. All new phases are calculated to be metastable, as they require a highly activated Nitrogen source with chemical potentials well above the thermodynamic N_2 gas phase. Effective N chemical potential up to about $\Delta\mu N \approx 1$ eV above the low-temperature limit of N_2 have been demonstrated before by sputtering deposition[8]. The trivalent Sb

nitride SbN becomes stable at $\Delta\mu N \geq +0.8$ eV, and, thus, might be synthesizable (efforts towards synthesis of SbN are ongoing and will be reported elsewhere). However, the pentavalent Sb_3N_5 requires $\Delta\mu N \geq +1.7$ eV and is likely out of reach, even for nonequilibrium thin-film synthesis.

As seen in the phase diagram in Fig. 1A, the spinel phase $ZnSb_2N_4$ shows a wide stability region among the ternary Zn-Sb nitrides. However, it requires very high $\Delta\mu N$, $\geq +1.0$ eV, across its entire space, suggesting that synthesis would be difficult, if possible at all. Thus, it could be challenging to synthesize it as phase-pure material. It is noticeable that the addition of Zn in the ternary strongly stabilizes the Sb +5 oxidation state, which is highly unstable as a binary Sb nitride. The relative stability of Zn_2SbN_3 also practically eliminates in the phase diagram the presence of ternary nitrides with Sb in the +3 state. Even though the third phase, Zn_3SbN_3 with Sb in the +3 state, has a similar critical $\Delta\mu N$, it has a very small stability window between Zn_2SbN_3, Zn_3N_2, and elemental Sb.

S2 – Experimental synthesis and characterization.

Experimental synthesis of Zn-Sb-N thin-film sample libraries was performed using combinatorial co-sputtering of Zn and Sb metals in the presence of N_2 on glass substrates in a deposition chamber with base pressure better than 1×10^{-6} Torr. Two sputtering guns were loaded with 2"-diameter Zn and Sb metal targets and positioned at 45° with respect to the substrate normal to achieve a cation compositional gradient. Both temperature and sputtering powers were varied to assess the effect of the deposition conditions on the properties of Zn_2SbN_3. Before the deposition, the 2"×2" Eagle-XG glass substrates were cleaned by degreasing in water and soap, followed by ultrasonic cleaning in acetone and isopropanol baths. The flow of the gases was set to 10 and 10 sccm for Ar and N_2, respectively. The sputtering pressure was adjusted between 20 and 10 mTorr, to change from more nitridizing to more reducing conditions during the growth. Spatially resolved characterization of the thin-film sample libraries was performed on a 4×11 grid of samples - 4 rows and 11 columns, with the compositional gradient along the 11 positions in one row. Compositional analysis was performed by both X-Ray Fluoresce in combinatorial mode and by Rutherford Back Scattering (RBS) on selected samples. For XRF, a Fischer Scientific (Fischerscope XDV-SDD) instrument using a spot size of 3 mm in diameter was used. Rutherford backscattering was performed using a model 3S-MR10 RBS system from National Electrostatics Corporation, with either high (168°, RBS) or low (110°, RBG) scattering angles. More information about the technique can be find elsewhere[1].

Structural characterization was performed using a Bruker D8 XRD in Cu Kα radiation, equipped with a two-dimensional (2-D) detector and a spot size on the order of 2 mm × 3 mm. For selected samples Structural characterization was performed using Beamline 11-3 at the Stanford Synchrotron Radiation Lightsource (SSRL) with an incident wavelength of 0.9744 Å. The experimental data were collected by

using a Rayonics 225 2D detector and the data range is 0.52 Å-1 ≤ q ≤ 5.40 Å-1. q was obtained by using the equation $q = \frac{4\pi}{\lambda}\sin\theta$, where λ is the incident wave length and θ is the diffraction angle. The integration and background removal were performed by using GSAS-II software.[9]

The optical transmittance and reflectance were measured in the wavelength range of 300−1700 nm on a home-built ultraviolet−visible light−near-infrared (UV-vis-NIR) spectrometer (no integrating sphere) with a spot diameter of ~1 mm. Electrical conductivity was measured using a custom four-point probe measurement instrument with tungsten probe spacing of 1 mm. The analysis of the characterization results was performed using custom-written procedures in the Wavemetrics IGOR Pro software package. The resulting data are available at htem.nrel.gov.

X-Ray Photoelectron Spectroscopy (XPS) and Ultraviolet Photoelectron Spectroscopy (UPS) was performed using a PHY-5600 system. A monochromatic Al k-alpha source was employed for the XPS measurements whereas a He(I) line was used for the UPS measurements.

XRD pattern as a function of cation composition plotted heat maps are reported in SI2, for some selected deposition conditions tested. As it can be seen, the crystallinity region is more extended for sample grown at 20 mTorr and at moderate temperature (200°C).

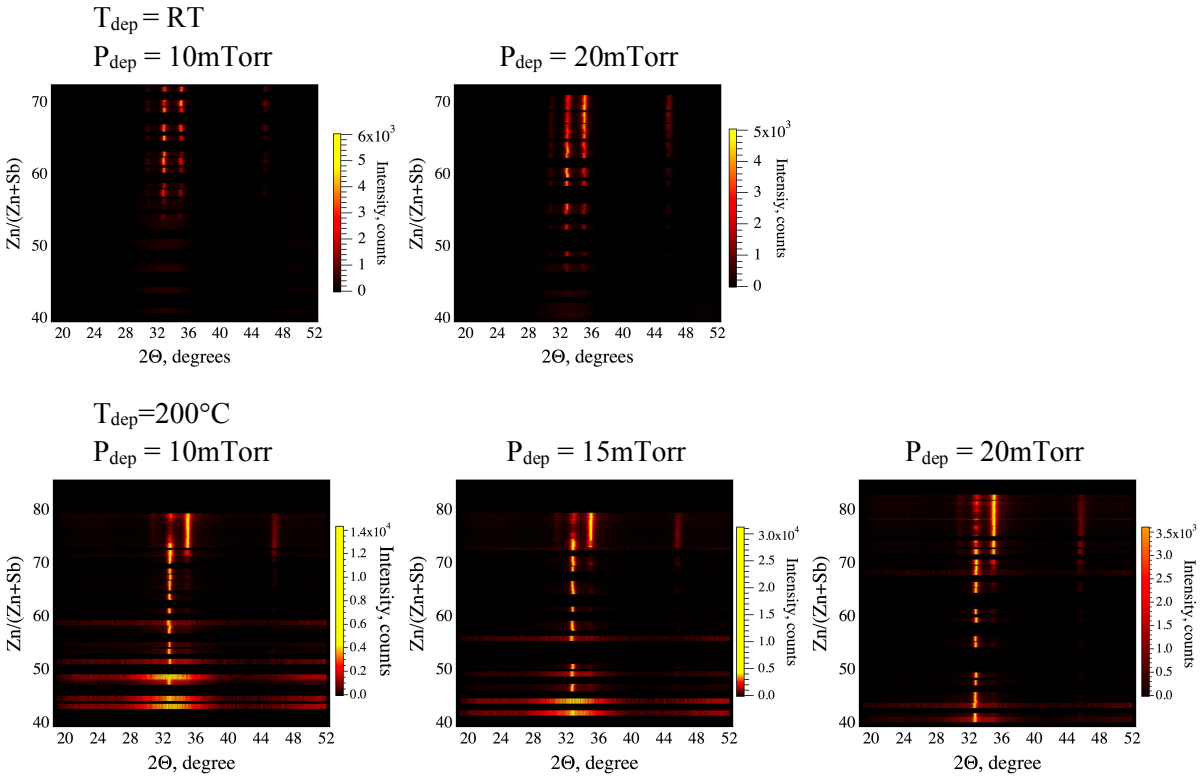

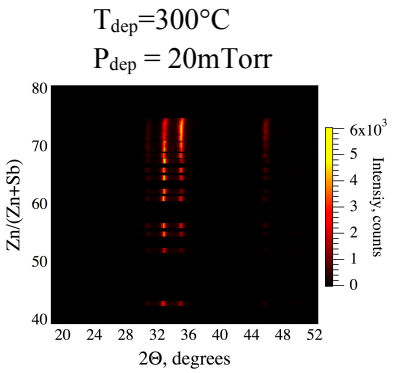

Figure SI 2. XRD patterns reported as heat maps for several deposition conditions tested

Table 1. Comparison between the cation composition determined by RBS and the XRF for a selected point in the library. The first two points (Row1-Column1, Row1-Column3 in the map where the columns are numbered 0 to 10) are composition outside of the crystallinity region.

Position	f_{Zn} RBS	f_{Zn} XRF	Full stoichiometry	Crystalline/Amorphous
R1C1	0.31	0.30	$Zn_{0.9}Sb_2N_{2.5}$	Amorphous
R1C3	0.35	0.37	$Zn_{1.1}Sb_2N_{3.4}O_{0.03}$	Amorphous
R1C5	0.63	0.65	$Zn_{1.7}SbN_3O_{0.28}$	Crystalline
R1C7	0.71	0.71	$Zn_{2.5}SbN_{3.7}$	Crystalline
R1C9	0.73	0.74	$Zn_{2.7}SbN_{3.8}$	Crystalline

The first two points were acquired in a portion of the sample which was Sb-reach, outside the crystallinity region identified by XRD. Thus, they refer to a part of the sample which was amorphous. The last three points were acquired at composition within the crystallinity range. The change from amorphous to crystalline is also accompanied with a drastic change in the elemental ratio, particularly the Zn/N content.

Selected samples were subject to RBS measurements to determine the nitrogen and oxygen content in the films and compared the cation composition determined by XRF with the value determined by RBS. Table S1 reports the values for one specific library where RBS was conducted on a spatially resolved manner. This analysis shows that the XRF determined values of cation composition were very accurate (within 1% of the values determined by RBS). Oxygen content in the films was very low, and it could be detected above the background signal only for few points in the sample. This is conducive of the that the oxygen content in the film is below 10%.

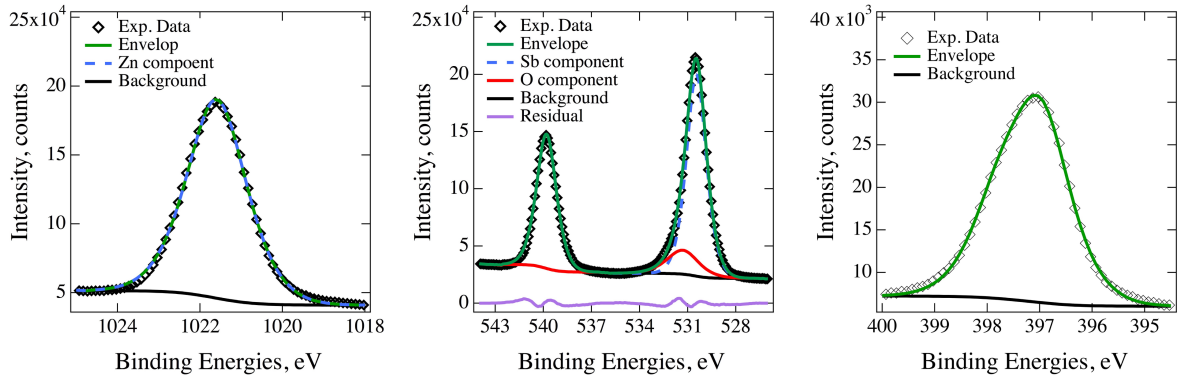

Figure SI 3. Core levels recorded for Zn, O and N respectively.

Figure SI3 reports the XPS spectra recorded on a film grown at room temperature and having composition f_{Zn} =0.65. The Zn $2p_{3/2}$, Sb 3d and N1s core levels are reported here. The $Sb3d_{5/2}$ core level of antimony is superimposed with the O 1s level. In order to separate the related contribution, peak fitting on the Sb 3d peaks was carried out using a tabulated spin orbit splitting separation between the Sb $3d_{5/2}$ and $3d_{3/2}$ and the ratio between the integrated area of 3:2. The residual on the peak positioned at ~531eV was fitted with a single component which is attributed to the O1s contribution. In order to assess whether $Zn(OH)_2$ was present at the surface, Zn-Auger lines were acquired during the survey. Based on the position of the Zn 2p core-level and the position of the Auger lines (Auger KE = 988.8 eV), we ruled out the presence of $Zn(OH)_2$ at the surface, however we cannot rule out the presence of a very small amount of ZnO.

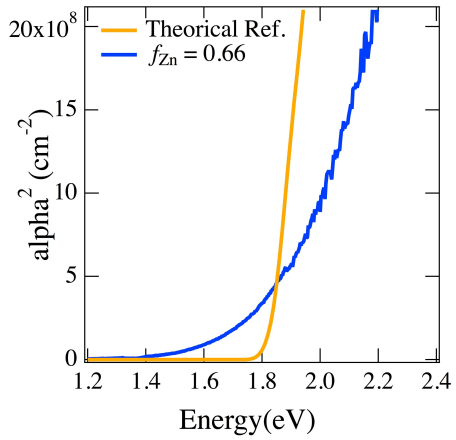

Figure SI 4. Squared value of the absorption coefficient plotted as a function of energy.

Optical spectra for a nearly stoichiometric films were recorded. In order to determine the position of the absorption onset, the absorption coefficient was plotted as squared function. For comparison the theoretical spectrum is reported as well. Whereas theory predicts a fundamental direct band gap of 1.71 eV, the absorption onset of these films is slightly more diffused and start at lower energies. This behavior has been observed in other materials which adopt the wurtzite derived structure and it is attributed to disorder on the cation sublattice.

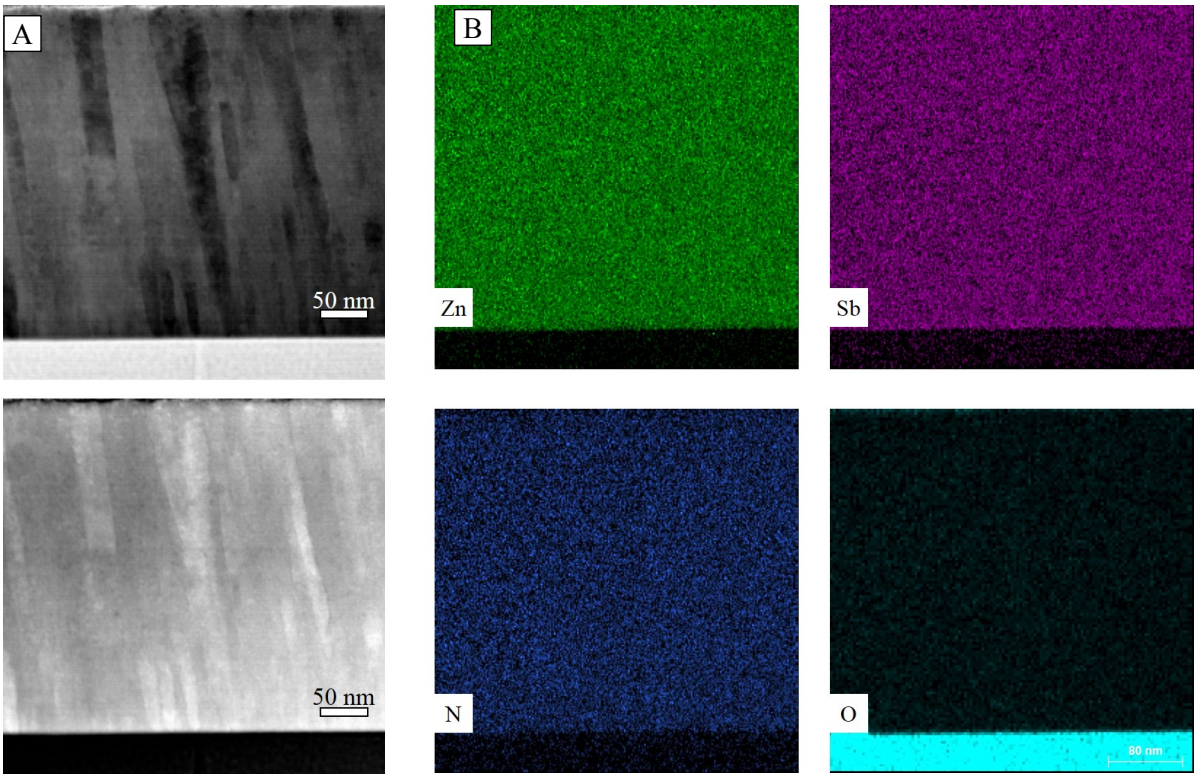

Figure SI 5. A) TEM and B) EDX mapping of a sample grown at room temperature.

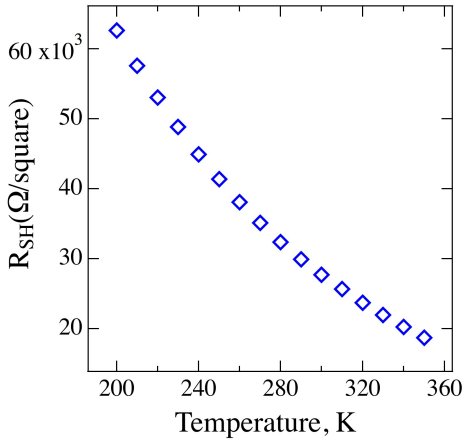

Figure SI 6. Sheet resistance measured as a function of temperature.

An example of the resistance vs temperature measurements is reported in Figure SI6. The temperature activated behavior indicates that Zn_2SbN_3 is a semiconductor.

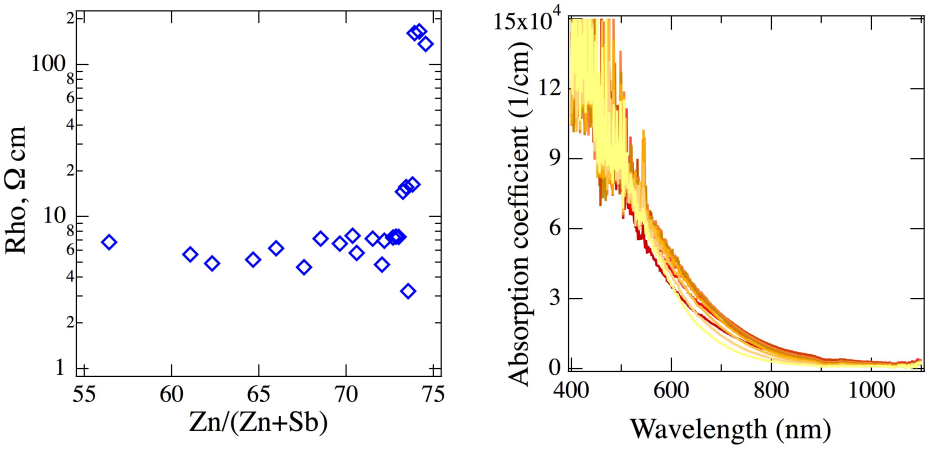

Figure SI 7 A) Resistivity and B) Absorption coefficient reported as a function of composition.

Figure SI7A reports the electrical measurements of two thin films measured grown at different substrate temperature as a function of composition: unintentional heat (RT temperature) and substrate temperature of 300°C. The resistivity of the sample increases substantially at the edge of the crystallinity region, having very small variation with composition within the crystallinity region and decreasing for samples deposited at moderate temperature. The absorption coefficient remains quite unchanged in the composition region spanning from f_{Zn} =0.8 to f_{Zn} =0.65

References

1. E. Arca, S. Lany, J. D. Perkins, C. Bartel, J. Mangum, W. Sun, A. Holder, G. Ceder, B. Gorman, G. Teeter, W. Tumas and A. Zakutayev, *Journal of the American Chemical Society*, 2018, **140**, 4293-4301.
2. H. T. Stokes and D. M. Hatch, *Journal of Applied Crystallography*, 2005, **38**, 237-238.
3. G. Kresse and D. Joubert, *Physical Review B*, 1999, **59**, 1758-1775.
4. M. Shishkin and G. Kresse, *Physical Review B*, 2006, **74**, 035101.
5. V. Stevanović, S. Lany, X. Zhang and A. Zunger, *Physical Review B*, 2012, **85**, 115104.
6. S. Lany, *Physical Review B*, 2013, **87**, 085112.
7. M. Gajdoš, K. Hummer, G. Kresse, J. Furthmüller and F. Bechstedt, *Physical Review B*, 2006, **73**, 045112.
8. C. M. Caskey, R. M. Richards, D. S. Ginley and A. Zakutayev, *Materials Horizons*, 2014, **1**, 424-430.
9. B. H. Toby and R. B. Von Dreele, *Journal of Applied Crystallography*, 2013, **46**, 544-549.